


Comment on “Fully gapped superconductivity and topological aspects of the noncentrosymmetric superconductor TaReSi”

Andrzej Ptok ^{*}

Institute of Nuclear Physics, Polish Academy of Sciences, W. E. Radzikowskiego 152, PL-31342 Kraków, Poland



(Received 28 July 2023; revised 17 April 2024; accepted 11 June 2024; published 24 June 2024)

In a recent paper [Shang *et al.*, *Phys. Rev. B* **107**, 224504 (2023)], the authors study the physical properties of TaReSi compounds having *Ima2* structure. This noncentrosymmetric structure is proposed to be the source of topological properties for the mentioned compound. However, for a correct description of topological features, it is important to recognize the correct structure of the compound at low temperatures. In this Comment, we show that *Ima2* cannot be realized by TaReSi and is unstable at low temperature. The *Ima2* structure contains the soft modes at the S (1/2, 0, 0) point, which leads to the stable structure with *Cm* symmetry. Notably, the stable *Cm* system also has a noncentrosymmetric structure, which can be the actual source of topological properties.

DOI: [10.1103/PhysRevB.109.216501](https://doi.org/10.1103/PhysRevB.109.216501)

In a recent paper Shang *et al.* [1] discuss the properties of the TaReSi compound, exhibiting the superconductivity below $T_c = 5.5$ K. The presented theoretical investigation is based on the assumption that this compound realizes an orthorhombic TiFeSi-like structure with *Ima2* symmetry (space group No. 46), presented in Fig. 1(a). This statement is supported by powder x-ray diffraction under normal conditions [2], i.e., temperatures much higher than the superconducting state. Nevertheless, the symmetry of TaReSi can differ in the low-temperature regime, which can affect the electronic and topological properties of this compound. In this Comment, based on the *ab initio* calculations, we discuss the stability of TaReSi in the range of low temperatures.

Computational details. The *ab initio* calculation within the density functional theory (DFT), were performed using the projector augmented-wave potentials [3] implemented in the Vienna *Ab initio* Simulation Package (VASP) code [4–6]. Calculations were made within the generalized gradient approximation in the Perdew, Burke, and Ernzerhof parametrization [7]. The energy cutoff for the plane-wave expansion was set to 350 eV. Optimizations of structural parameters (lattice constants and atomic positions) were performed in the primitive unit cell using the $10 \times 10 \times 6$ **k**-point grid in the Monkhorst-Pack scheme [8]. As a break of the optimization loop, we take the condition with an energy difference of 10^{-6} and 10^{-8} eV for ionic and electronic degrees of freedom. The optimized system symmetry was analyzed using FINDSYM [9].

The dynamical properties were calculated using the direct Parlinski-Li-Kawazoe method [10], implemented in the PHONOPY package [11,12]. Within this method, the interatomic force constants were calculated from the forces acting on the atoms after displacement of individual atoms inside a supercell. We performed these calculations using the supercell

containing $2 \times 2 \times 2$ conventional cells, which corresponds to 48 formula units, and a reduced **k**-grid of $3 \times 3 \times 3$.

Stability of TaReSi at low temperatures. The phonon dispersion curves for symmetry *Ima2* are presented in Fig. 1(c). As we can see, within the phonon spectrum there exists an imaginary soft mode (presented as negative frequencies), which indicated the dynamical instability of TaReSi with

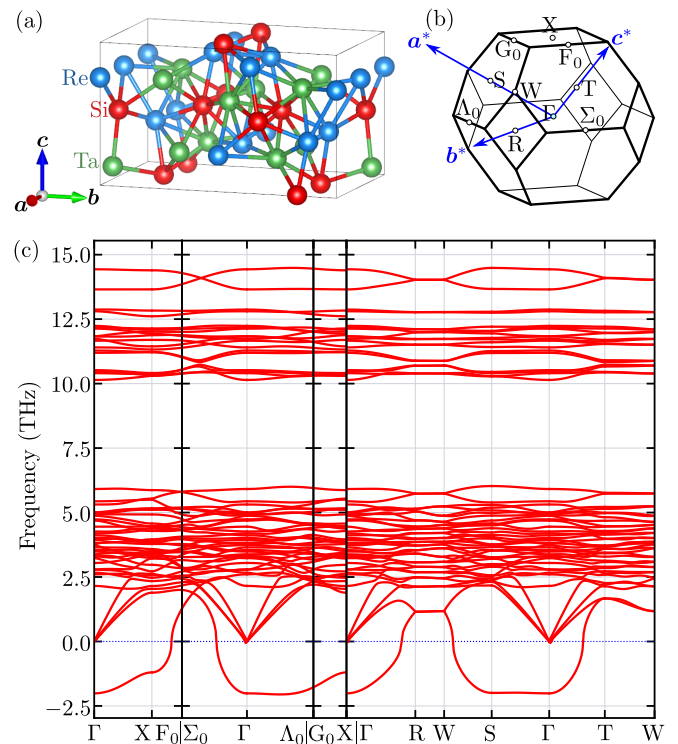


FIG. 1. (a) Conventional unit cell of TaReSi with *Ima2* symmetry and (b) correspondingly the Brillouin zone with its high-symmetry points. (c) Phonon dispersion curves for TaReSi with *Ima2* symmetry.

^{*}Contact author: aptok@mmj.pl

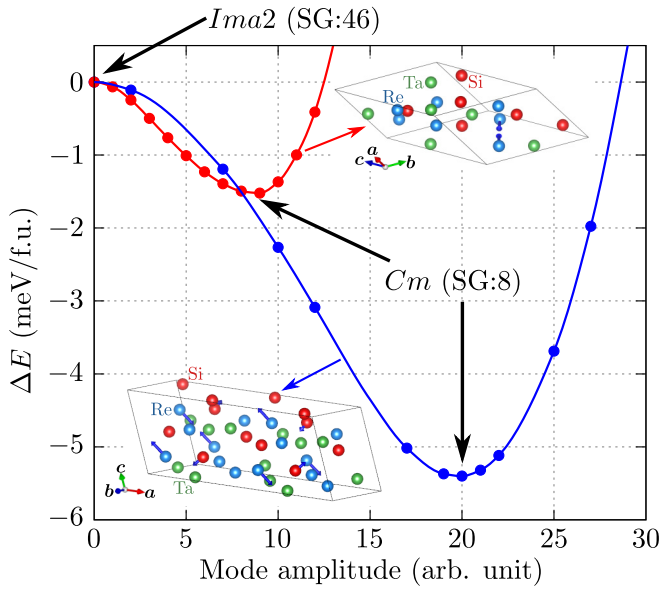


FIG. 2. Total energy (per formula unit) of TaReSi as a function of the soft mode amplitude. Red and blue colors correspond to the displacement generated by the soft mode at Γ and S points, respectively (see Fig. 1). The relative energies of the initial $Ima2$ and final structures (both with Cm symmetry) are indicated by arrows. Insets show the crystal structure and the atom displacement (blue arrows) introduced by the discussed soft modes.

$Ima2$ at low temperatures. However, the atom displacement induced by the soft modes can be used to predict the *true* group state of the system. In this Comment, we present analyses of the possible stable structure of TaReSi at low temperature.

For further analysis, we take soft modes at Γ (0, 0, 0) and S ($1/2, 0, 0$) points (i.e., soft modes with the largest magnitude of frequencies). First, it should be noted, that the soft mode from the Γ point does not change the size of the primitive unit cell, while the one at the S point leads to its doubling along the lattice vector a . The displacement of the atoms introduced by the soft modes should lead to new structures with a total energy lower than that of the $Ima2$ structure. Indeed, the introduction of atom displacement induced by both soft modes leads to energy lowering, which is clearly seen in Fig. 2.

The symmetries of the structures induced by both soft modes (before and after structure optimization) are recognized as Cm structures (space group no. 8) (details about the optimized structure can be found in the Supplemental Material (SM) [13]). Unfortunately, the displacements of the atoms are related to the entire structure of the compound. In the case of the soft mode at the Γ point (red line in Fig. 2), the energy of the system is minimized by the structure when the atoms of Ta, Re, and Si are shifted by 0.025, 0.101, and 0.046 Å, respectively. Similarly, for the displacement of atoms induced by the soft mode at the S point (blue line in Fig. 2), these values are 0.061, 0.153, and 0.098 Å, for Ta, Re, and Si atoms, respectively.

In order to investigate the dynamical stability of the “new” structure, we reanalyzed the corresponding phonon spectra. The phonon dispersion curves for the structure induced by

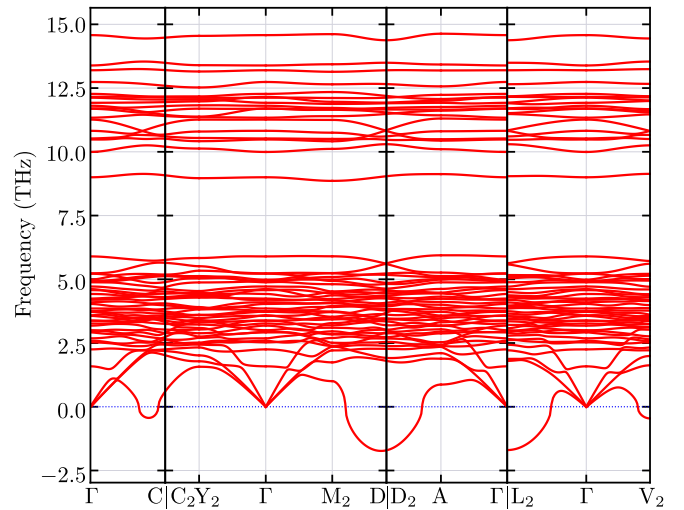


FIG. 3. Phonon dispersion curves for TaReSi with Cm symmetry induced by the soft mode at the Γ point (see Fig. 1).

the soft mode at the point Γ are presented in Fig. 3. In this case, the phonon spectra still possess the soft mode, which is expected in the context of the result presented in Fig. 2—there is structure (induced by the soft mode from the S point) with lower energy. In the case of this structure, the phonon spectra do not exhibit any imaginary soft modes (Fig. 4), and the structure is stable in the dynamical sense.

In the optimized (stable) structure of TaReSi with Cm symmetry, the atoms are located in 26 nonequivalent positions (see crystal structures in the SM [13]): Ta, Re, and Si atoms contain 12, 6, and 8 nonequivalent positions, respectively. Interestingly, Ta atoms are located only in $2a$ Wyckoff positions and Re atoms are located only in $4b$ positions, while Si atoms are contained in both $2a$ and $4b$ positions. As a result, a conventional unit cell contains 24 formula units, which correspond to two primitive unit cells. Similarly to the case of the previously discussed unstable $Ima2$ structure [1], a stable Cm structure is

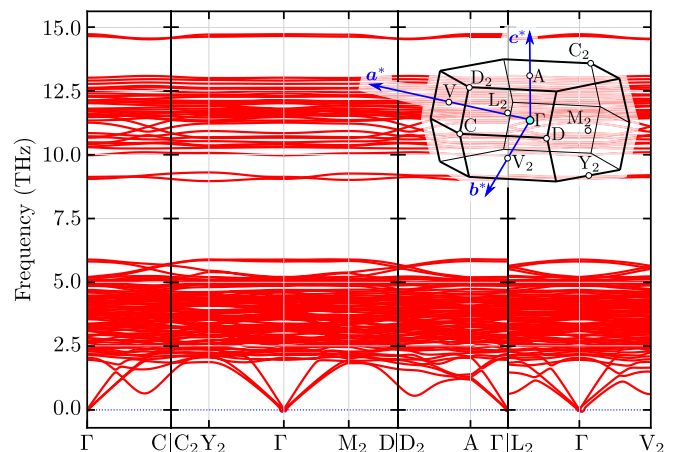


FIG. 4. Phonon dispersion curves for TaReSi with Cm symmetry induced by the soft mode at the S point (see Fig. 1). Inset shows the Brillouin zone and its high-symmetry points.

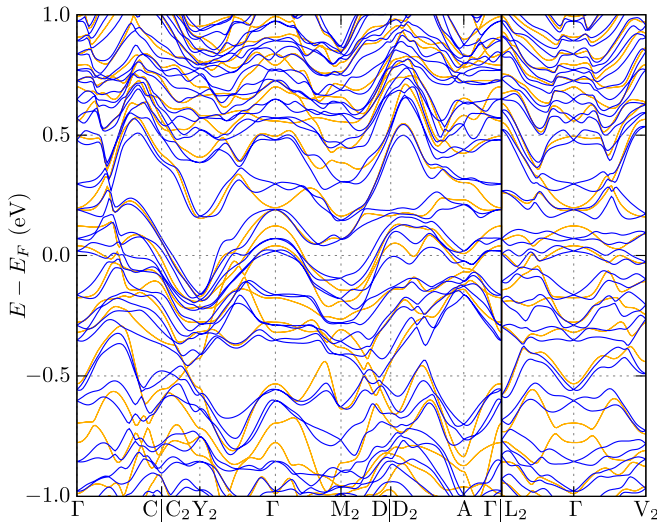


FIG. 5. Electronic band structure of TaReSi with C_m symmetry (induced by the soft mode originated at the S point). Orange and blue lines correspond to the band structure in the spin-orbit-coupling absence and presence, respectively.

noncentrosymmetric, which allows for the realization of the antisymmetric spin-orbit coupling [14].

The presented situation can be compared with NbReSi, which is reported as $Ima2$ [15] or $P\bar{6}2m$ [16–18] structure. In this case, there is also a soft mode for $Ima2$, and, undoubtedly, the system forms a $P\bar{6}2m$ structure [19]. Contrary to this, TaReSi is recognized as $Ima2$ under normal conditions, whereas the existing soft mode leads to the stable C_m symmetry in the case of the low-temperature regime.

Electronic properties. Finally, for the optimized stable C_m structure, we can calculate the electronic band structure (Fig. 5). The lifting of the band degeneracy by the spin-orbit coupling is well visible (cf. orange and blue lines in Fig. 5). The calculated band splitting for the C_m structure (600 meV) is much greater than that reported for the $Ima2$ structure (300 meV) [1]. In the presence of the spin-orbit coupling (blue lines in Fig. 5), the electronic band structure hosts the double degenerate Weyl points. It is worth noting that for the $Ima2$ symmetry [1], there are no Kramers nodal lines along the high-symmetry lines. Nevertheless, the existence of the mirror symmetry plane $\{m_{010}|0\}$ within the C_m symmetry allows for realization of the Kramers nodal lines in the mirror planes. Such nodal lines create the close contours between the high-symmetry points Γ , A, M, and Y (represented by the black

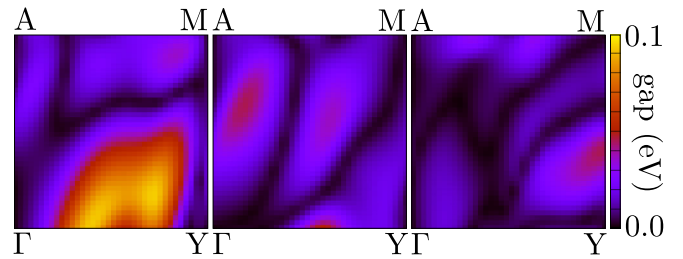


FIG. 6. The value of the “gap” between pairs of bands splitting by the spin-orbit coupling. Black lines suggest the realization of the Kramers nodal lines. Results for three pairs of bands crossing the Fermi level for a plane in the Brillouin zone (Γ -A-M-Y plane).

contours on Fig. 6). The vanishing band splitting (no-gap) between pairs of bands splitting by the spin-orbit coupling is clearly visible and is not limited to the high-symmetry points [20].

Summary and conclusions. In this Comment, based on the DFT calculations, we establish that the TaReSi in the low-temperature range cannot form a stable structure with $Ima2$ symmetry. This is based on the fact that the phonon spectra calculated for $Ima2$ TaReSi contain the imaginary-frequency soft modes. The precise examination of the realized symmetry is necessary for a discussion of the TaReSi topological properties, which is the main intent of the presented Comment.

Here, we display the calculation suggesting that the C_m structure is more preferable in low-temperature regime. TaReSi with C_m symmetry is still noncentrosymmetric, which is related to the existence of antisymmetric spin-orbit coupling, as claimed in Ref. [1]. Additionally, the spin-orbit-coupling strength for C_m symmetry is much larger than the one reported for $Ima2$, which indeed can support the realization of the topological superconductivity in TaReSi [1]. The absence of inversion symmetry, while preserving mirror symmetry, is a source of Kramers nodal lines [20]. In such a case, the vanishing of the band splitting introduced by the spin-orbit coupling forms the closed contours between high-symmetry points. The close vicinity of this band crossing to the Fermi level can be of importance for the topological properties of TaReSi at low temperatures, as reported by experimental observation in Ref. [1].

Acknowledgments. Some figures in this work were rendered using VESTA [21] software. A.P. is grateful to Laboratoire de Physique des Solides in Orsay (CNRS, University Paris Saclay) for hospitality during the work on this project. This work was supported by the National Science Centre (NCN, Poland) under Project No. 2021/43/B/ST3/02166.

[1] T. Shang, J. Z. Zhao, L.-H. Hu, D. J. Gawryluk, X. Y. Zhu, H. Zhang, J. Meng, Z. X. Zhen, B. C. Yu, Z. Zhou, Y. Xu, Q. F. Zhan, E. Pomjakushina, and T. Shiroka, Fully gapped superconductivity and topological aspects of the noncentrosymmetric superconductor TaReSi, *Phys. Rev. B* **107**, 224504 (2023).
 [2] K. P. Sajilesh and R. P. Singh, Superconducting properties of the non-centrosymmetric superconductors TaXSi ($X = \text{Re}, \text{Ru}$), *Supercond. Sci. Technol.* **34**, 055003 (2021).

[3] P. E. Blöchl, Projector augmented-wave method, *Phys. Rev. B* **50**, 17953 (1994).
 [4] G. Kresse and J. Hafner, *Ab initio* molecular-dynamics simulation of the liquid-metal–amorphous-semiconductor transition in germanium, *Phys. Rev. B* **49**, 14251 (1994).
 [5] G. Kresse and J. Furthmüller, Efficient iterative schemes for *ab initio* total-energy calculations using a plane-wave basis set, *Phys. Rev. B* **54**, 11169 (1996).

- [6] G. Kresse and D. Joubert, From ultrasoft pseudopotentials to the projector augmented-wave method, *Phys. Rev. B* **59**, 1758 (1999).
- [7] J. P. Perdew, K. Burke, and M. Ernzerhof, Generalized gradient approximation made simple, *Phys. Rev. Lett.* **77**, 3865 (1996).
- [8] H. J. Monkhorst and J. D. Pack, Special points for Brillouin-zone integrations, *Phys. Rev. B* **13**, 5188 (1976).
- [9] H. T. Stokes and D. M. Hatch, FINDSYM: program for identifying the space-group symmetry of a crystal, *J. Appl. Cryst.* **38**, 237 (2005).
- [10] K. Parlinski, Z. Q. Li, and Y. Kawazoe, First-principles determination of the soft mode in cubic ZrO_2 , *Phys. Rev. Lett.* **78**, 4063 (1997).
- [11] A. Togo, First-principles phonon calculations with PHONOPY and PHONO3PY, *J. Phys. Soc. Jpn.* **92**, 012001 (2023).
- [12] A. Togo, L. Chaput, T. Tadano, and I. Tanaka, Implementation strategies in PHONOPY and PHONO3PY, *J. Phys.: Condens. Matter* **35**, 353001 (2023).
- [13] See Supplemental Material at <http://link.aps.org/supplemental/10.1103/PhysRevB.109.216501> for the crystallographic information file (CIF) for optimized structures with Cm symmetry.
- [14] M. Smidman, M. B. Salamon, H. Q. Yuan, and D. F. Agterberg, Superconductivity and spin-orbit coupling in non-centrosymmetric materials: a review, *Rep. Prog. Phys.* **80**, 036501 (2017).
- [15] S. K. P., K. Motla, P. K. Meena, A. Kataria, C. Patra, S. K., A. D. Hillier, and R. P. Singh, Superconductivity in noncentrosymmetric NbReSi investigated by muon spin rotation and relaxation, *Phys. Rev. B* **105**, 094523 (2022).
- [16] H. Su, T. Shang, F. Du, C. F. Chen, H. Q. Ye, X. Lu, C. Cao, M. Smidman, and H. Q. Yuan, NbReSi: A noncentrosymmetric superconductor with large upper critical field, *Phys. Rev. Mater.* **5**, 114802 (2021).
- [17] T. Shang, D. Tay, H. Su, H. Q. Yuan, and T. Shiroka, Evidence of fully gapped superconductivity in NbReSi: A combined μSR and NMR study, *Phys. Rev. B* **105**, 144506 (2022).
- [18] S. Nandi, S. Sasmal, B. B. Maity, V. Sharma, G. Dwari, R. Kulkarni, and A. Thamizhavel, Anisotropic properties of a noncentrosymmetric NbReSi superconducting single crystal, *Phys. Rev. B* **107**, 134518 (2023).
- [19] S. Basak and A. Ptok, Theoretical study of dynamical and electronic properties of noncentrosymmetric superconductor NbReSi, *Materials* **16**, 78 (2023).
- [20] Y.-M. Xie, X.-J. Gao, X. Y. Xu, C.-P. Zhang, J.-X. Hu, J. Z. Gao, and K. T. Law, Kramers nodal line metals, *Nat. Commun.* **12**, 3064 (2021).
- [21] K. Momma and F. Izumi, VESTA3 for three-dimensional visualization of crystal, volumetric and morphology data, *J. Appl. Cryst.* **44**, 1272 (2011).